DOI: 10.13009/EUCASS2025-605
11TH EUROPEAN CONFERENCE FOR AERONAUTICS AND SPACE SCIENCES (EUCASS)

Global plasma modeling of an Argon and Helium fed Microwave Electrothermal Thruster operating at kilowatts power levels

Michele Lauriola[1†], *Michele Nava*[2], *Alessandro Maffini*[1], *Filippo Maggi*[2] *and Matteo Passoni*[1]
[1]*Department of Energy, Politecnico di Milano, Milan (Italy) 20156*
[2]*Department of Aerospace Science and Technology, Politecnico di Milano, Milan (Italy) 20156*
michele.lauriola@polimi.it · michele1.nava@polimi.it
[†]Corresponding author

Abstract

The Microwave Electrothermal Thruster (MET) is an electrodeless device using microwaves, and a free-floating plasma, to heat a propellant which expands through a solid nozzle. This simple, scalable thruster is compatible with many propellants, and offers extended lifetime over mature technologies.
This study develops a self-consistent MET global (volume-averaged) model working with argon and helium. The model predicts the plasma parameters, the wall temperature, and thruster performances (thrust, specific impulse, efficiency). Input powers of 1 and $2\,kW$ and mass flow rate up to $2\,g/s$ are explored. Results show that helium has greater performance whereas argon has high power reflection, reducing the thruster efficiency. The model enables rapid performance estimation across various conditions, at low computational cost, supporting thruster design and optimization.

1. Introduction

Electric thrusters use electrical energy to energize a propellant, by means of a plasma (a gas of interacting charged and neutral species that responds to electromagnetic fields). This allwows them to achieve higher exhaust velocities than chemical thrusters, improving the propellant mass economy.[14]
Although many EP technologies have reached a high maturity level (e.g., Hall Effect Thruster, Gridded Ion Engine, Arcjet) and are employed in several missions,[12] they use electrodes and grids sensitive to the high plasma fluxes impinging on them, causing lifetime limitation and performance degradation. The electrodeless plasma trhuster paradigm attempts to overcome these limitations by removing the critical elements.[14]
The Microwave Electrothermal Thruster (MET) has emerged among the electrodeless technologies for its technological simplicity and high versatility.[5,15] In a MET, microwaves generate a free-floating plasma that heats a swirling propellant, which then expands through a nozzle to produce thrust. In addition to being simple, this thruster is highly scalable,[15] compatible with many propellants,[5,7,8] and it has performance comparable to that of arcjets. However, research is still ongoing in research institutions.
Over the years, MET fluid and electromagnetic numerical models have been used to study the plasma discharge, the electromagnetic field distribution inside the chamber, and to design and optimize the thruster.[11,15,21] However, simulations can be computationally demanding and time-consuming, taking hundreds of hours to reach a steady-state solution with atomic gases,[11] and limiting the thruster analysis across a broad range of parameters (e.g., dimensions, input power, mass flow rate).
Global (0D) plasma models are a subclass of fluid models which compute volume-averaged physical quantities, such as plasma species densities and temperatures. They are especially useful for modeling systems with complex chemistry, investigating the effects of several external parameters, and identifying relationships among them without the long computational times required by spatially resolved models. Therefore, 0D models serve as a fast and predictive tool to investigate the system behavior and performance, providing guidance for more complex models and/or experiments.
To the author's knowledge, only a few MET global plasma models can be found in the literature.[4,20,23] However, they lack a fully self-consistent description of the plasma and thruster systems. In fact, they do not describe propellant heating treating its temperature as an input[23] or neglect heat transfer to the wall.[4,20] However, accurately accounting for power losses to the walls is essential both for quantifying the overall MET efficiency and for estimating the wall temperature. These factors are critical in identifying optimal operating conditions and selecting wall materials.

DOI: 10.13009/EUCASS2025-605

Therefore, this study aims at developing a MET global plasma model that includes two additional power balance equations describing gas and wall temperature heating. The model has been applied to atomic gas propellants, such as argon and helium, because they are commonly used in experiments and in simulations. It computes steady-state plasma parameters, i.e., species densities, electron temperature, and heavy species temperature, and the wall temperature while varying input power and mass flow rate across a wide range. These values are then used to predict the MET propulsive performance, i.e., thrust, specific impulse, and thrust efficiency.
Section 2 describes the MET and its worrking principle. Section 3.1 is entirely dedicated to the description of the developed MET (0D) model. The main parameters used in the simulations performed are presented in section 4 while results and their discussion are provided in section 5. Finally, section 6 presents the conclusions and outlines the key open points and possible future directions of this work.

2. The Microwave Electrothermal Thruster

The Microwave Electrothermal Thruster (MET) is an electrothermal and electrodeless consisting of a cylindrical resonant cavity whose dimensions depend on the frequency of the resonant mode chosen according to the well-known electromagnetic theory, and is divided by a dielectric separation plate into an *antenna* and a *plasma* section.[10,15] The former hosts the antenna, feeding the microwave power into the thruster, and is constantly kept at atmospheric pressure to prevent plasma formation. In the latter section, the propellant is injected and the plasma is ignited. Additionally, one side is enclosed by an endplate housing the nozzle.[15]
MET operation[15] starts with the excitation of a TM_{011} mode within the cavity, which permits to maximize the electric power density on the axis and near the nozzle inlet. Then, the propellant is injected, a microwave breakdown occurs, and a plasma is formed. Plasma electrons can now absorb microwave energy and transfer it to the heavy species through a series of elastic collisions, increasing their thermal energy. Finally, the heated gas is accelerated by passing through a convergent-divergent nozzle, producing thrust. Figure 1 represents a simple scheme of the MET chamber and its working principle. The MET was efficiently tested and modeled in a broad range of input power, from a few watts[6,11] to kilowatt power levels.[5,10,20] The MET can also work with several propellants: argon,[22] helium,[8] xenon,[17] nitrogen (N_2),[8] hydrogen (H_2),[18] hydrazine (N_2H_4),[7] ammonia (NH_3),[7] nitrous oxide (N_2O),[4,8] and water (H_2O).[5,8]

3. The global plasma model

MET global modeling offers a simplified approach to study and analyze the plasma behavior inside the chamber, gas heating, and the partitioning of input power among various plasma processes.[1,4,9] It is extremely useful to study plasmas with complex chemistry, with a large number of species and reactions, and to investigate how the plasma parameters change when operating conditions, e.g., input power, and external parameters are modified, keeping the computational time low (within minutes). The model consists of a set of coupled particle (PaBE) and power (PoBE)

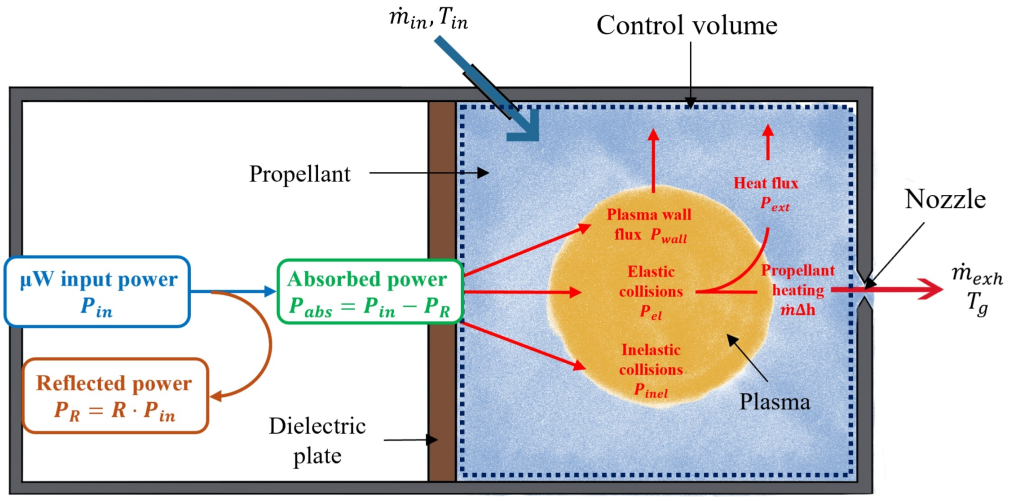

Figure 1: Simple MET scheme describing the geometry of the chamber and the main components alongside with a basic scheme of its working principle and the power partitioning. The control volume employed in the 0D model is also showed (It should be noted that it is limited to only the *plasma zone*, hosting the plasma).

DOI: 10.13009/EUCASS2025-605

balance equations, whose solution is the set of volume-averaged and time-dependent (or steady state) plasma species densities and temperatures.
The equations used are described hereafter: section 3.1 is devoted to the PaBE, while sections 3.2.1 and 3.2.2 to the two PoBEs.

3.1 Particle balance equations

The particle balance equation describes the change in species j number density, n_j, due to atomic and chemical reactions, or particle flowing into and out of the MET control volume:[1,9]

$$\frac{dn_j}{dt} = G_j - L_j + \sum_i \chi_{i,j} K_{i,j} \prod_l n_l^{\alpha_{i,l}} \tag{1}$$

where G_j (L_j) is the density change caused by a physical flow, e.g., gas inlet. The third term represents the species j production ($\chi_{i,j} > 0$) and loss ($\chi_{i,j} < 0$) due to reactions, where $\chi_{i,j}$ is the net stoichiometric coefficient for species j involved in reaction i, $K_{i,j}$ is the i-th reaction rate constant, n_l is the density of the l-th reactant involved and $\alpha_{i,l}$ is the related stoichiometric coefficient. Expressions for the rate constant $K_{i,j}$ can be found in the literature. Reaction rates for backward reactions can be computed using the principle of detail balance.
Neutral particles can leave the MET volume through the nozzle, with throat area A_T. This process can be modeled through a first-order loss rate, derived from the chocked mass flow rate computed using the quasi one-dimensional isentropic theory[19] $K^n_{exh,j} = \dot{m}_{exhaust,j}/(M_j n_j V)$, where $\dot{m}_{exhaust,j}$ is the neutral species j (choked) mass flow rate through a nozzle with throat area A_T.
The effect of diffusion and losses to the wall should be taken into account too. These processes include ion-electron recombination, or quenching of excited state at the cavity wall.[13] Mathematically, they can be modeled by reaction rates $K^{loss}_{W,j}$. Expressions for these can be found in the literature[4,13] and differ between neutral and charged species due to ambipolar diffusion. No PaBE is solved for the electron population because the electron density is calculated by imposing the plasma quasi-neutrality condition:

$$n_e = \sum_j Z_j n_j^{(+)} \tag{2}$$

where Z_j represents the species j charge state and it can be either positive or negative.

3.2 Power balance equations

In microwave plasmas, only electrons are directly heated by the electromagnetic field while the high elastic collision frequency can lead to substantial gas heating[16] resulting in a non-local thermodynamic equilibrium. Therefore, two PoBE modeling the electron and heavy species heating are necessary. Instead, ions are assumed to be in thermal equilibrium with the neutrals.

3.2.1 Electron power balance

The electron PoBE is:[1,9,13]

$$\begin{aligned}\frac{d}{dt}\left(\frac{3}{2} n_e k_B T_e\right) = \frac{P_{abs}(t)}{V} + \sum_j K_j^{inel} \prod_l n_l^{\alpha_{j,l}} \Delta E_j^{inel} - \sum_{j \in ion(+)} K^+_{W,j} n_j E_W + \\ - \sum_j \frac{3m_e}{M_j} K^{el}_{e,j} n_j n_e (T_e - k_B T_g)\end{aligned} \tag{3}$$

where P_{abs} is the fraction of input power absorbed by electrons, accounting for wave reflection. The second term on the RHS models the energy that electrons gain or loose due to inelastic collisions (e.g., ionization, excitation), with K_j^{inel} the reaction rate and ΔE_j^{inel} the associated reaction energy (negative if the electron looses energy). Values of these energy can be found in the literature. The third term describes the power lost at the boundary due to electrons striking the wall and E_W is the energy lost in the process, $E_W = 2T_e + |\Phi_{PS}| + |\Phi_W|$, where $2T_e$ is the average electron kinetic energy lost , $|\Phi_{PS}| = T_e/2$ is the energy lost in the pre-sheath, and $|\Phi_W|$ is the sheath potential drop contribution.[13] Finally, the last term model the energy exchange between electrons and heavy species through elastic collisions.
A plasma can reflect a fraction of the incident electromagnetic wave. The phenomenon can be mathematically modeled introducing a reflection coefficient Γ_ω depending on the wave frequency, the plasma density, and the collision

DOI: 10.13009/EUCASS2025-605

frequency.[3] An analytical expression of the reflection coefficient can be derived solving the wave equation with appropriate boundary conditions at a plasma-air interface. The power absorbed by the plasma can now be computed as $P_{abs} = P_{in}\,(1 - \Gamma_\omega)$.

3.2.2 Heavy species power balance

The heavy species power balance equation[2,4] is:

$$\frac{\mathrm{d}\,(\rho \mathrm{u})}{\mathrm{dt}} = \sum_j \frac{3m_e}{M_j} K_{e,j}^{el} n_j n_e (T_e - k_B T_g) V + \dot{m}\,(h_{in} - h_{exh}) - P_{ext} \tag{4}$$

where $\rho = \sum n_i M_i$ is the mixture density, $u = \sum Y_i u_i$ is the mixture specific energy, u_i and Y_i the species i specific energy and mass fraction, respectively. $\dot{m}$ is the mass flow rate (assuming mass conservation $\dot{m}_{in} = \dot{m}_{out} = \dot{m}$), $h = \sum Y_i h_i$ is the mixture specific enthalpy, while subscripts *in* and *exh* suggest that the summation should cover only those species entering the chamber and being exhausted through the nozzle, respectively.
P_{ext} is the rate of heat transferred to the external environment. An approximate expression of this term can be obtained by integrating Fourier's law[2] under the hypothesis of radial heat conduction, constant volumetric power generation, and temperature-independent heat conductivity.
Finally, a modified lumped capacitance model[2] was included to model wall temperature heating resulting form the incoming heat flux and radiated heat transfer to vaccum at $0\,K$.

4. Simulation setup

In all simulations, the cavity is assumed to work at a resonant frequency of $2.45\,GHz$, corresponding to a radius $5\,cm$ and a length $17.5\,cm$, and with a nozzle throat radius $r_T = 0.7\,mm$ (compatible with the dimensions of[20,23]). Cavity walls are assumed to be stainless steel, with a thickness $10\,\%$ of the cavity radius. For the sake of simplicity, material properties are kept constant and independent of temperature: thermal conductivity $\lambda_W = 15\,W/(m\,K)$ and emissivity $\epsilon = 0.5$. Finally, the inlet propellant temperature is kept at $300\,K$.
The studied mass flow rate ranges from $10\,mg/s$ to $5\,g/s$. Input powers of $1\,kW$ and $2\,kW$ are investigated.
For both argon and helium, only three species (X, X^+, e, $X = \{Ar, He\}$), and five reactions, listed in table 1, are considered, making the model very simple from a plasma chemical point of view. Electron-impact excitation was only included in the electron PoBE, and treated as an energy sink.

Table 1: Relevant reactions considered in the model, showing only the reaction type and its representation.

Electron-impact ionization	$e + A \rightarrow 2e + A^+$
Electron-impact excitation	$e + A \rightarrow e + A^*$
Electron-neutral elastic scattering	$e + A \rightarrow e + A$
Electron-ion elastic scattering	$e + A^+ \rightarrow e + A^+$
Wall recombination	$A^+ + \text{wall} \rightarrow A$
Neutral exhaust	–
Ion exhaust	–

The set of five ordinary differential equations (two PaBEs, the electron PoBE, the heavy species PoBE, and the wall temperature model), coupled to the quasi-neutrality condition and the wave power balance, is solved in steady-state for the neutral gas density n_g, the ion density n_i, the electron temperature T_e, the propellant temperature T_g, and the inner wall temperature T_w (wall temperature from now on).
Finally, thrust (F_T), specific impulse (I_{SP}), and thruster efficiency (η_T) (i.e., MET propulsive performance) are computed from these data. Quasi-1D isentropic theory[19] is used in the calculations, assuming the maximum theoretical velocity, v_{exh}^{max} is employed. In order to avoid thruster efficiencies larger than $100\,\%$, the cold thrust contribution is subtracted. The equations used are:

$$F_T = \sum_j \dot{m}_{j,exh}\, v_{j,exh}, \quad I_{SP} = \frac{F_T}{\dot{m}\, g_0}, \quad \eta_T = \frac{F_T^2 - F_{cold}^2}{2\dot{m}\, P_{in}}, \quad v_{exh,j}^{max} = \sqrt{\frac{2\gamma_{sh,j}}{\gamma_{sh,j} - 1} \frac{k_B T_g}{M_j}} \tag{5}$$

DOI: 10.13009/EUCASS2025-605

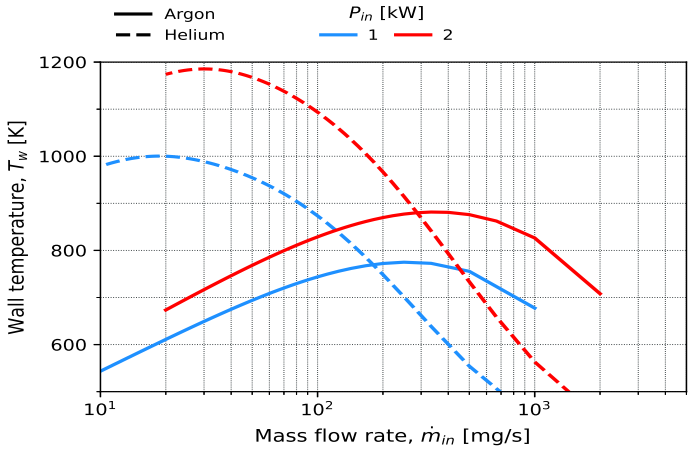

Figure 2: Computed chamber wall in argon (solid line) and helium (dashed line) plasma for input power $1 - 5\,kW$.

where the sum in the thrust definition covers only the species being exhausted through the nozzle, g_0 is the standard gravity acceleration, F_{cold} is the cold thrust, M_j is the species j particle mass in kilograms, and k_B is the Boltzmann's constant.

5. Results and discussion

Figure 2 presents the wall temperature as function of the mass flow rate. At low mass flow rate, the wall temperature in the helium-fed MET exceeds that of argon-fed MET, whereas the trends reverses at high flow rate. In both argon and helium plasmas, all curves exhibit a similar non-monotonic behavior and show the presence of a peak temperature (despite the peak is more pronounced in argon than in helium). Finally, wall temperature also increases with input power because of additional wall heating.

These non-monotonic trends are likely the result of combined increased power reflections and thermal losses. Figure 3 shows the absorbed power density (Figure 3a) and the heat fluxes (Figure 3b). As the input flow rate increases, the absorbed power rises, causing the wall temperature and the heat flux directed to the wall to increase. Additionally, when the input power is doubled, both the absorbed power density and the heat fluxes increases as well, consistently with equation 4. However, beyond a certain point, the heat fluxes diminish, leading to lower wall temperatures. At high flow rates, the heat fluxes in the helium plasma are lower than those in argon, resulting in a reduced wall temperature.

Figure 4 presents the thruster performance. Figure 4a displays the specific impulse as a function of the thruster-to-power ratio. According to Equation 5, the specific impulse should be inversely proportional to the thrust-to-power ratio. However, this trend is not observed at low thrust-to-power ratios (i.e., at high mass flow rate) due to the non-

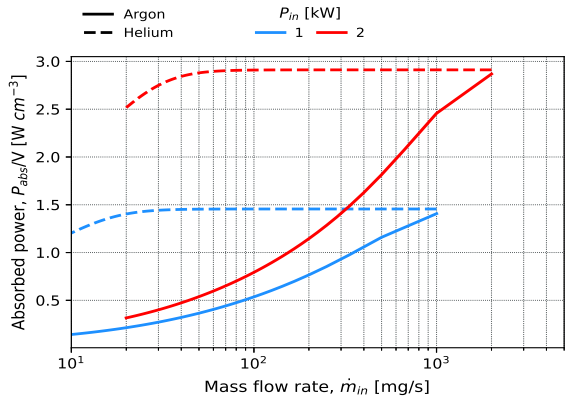

(a) Argon plasma.

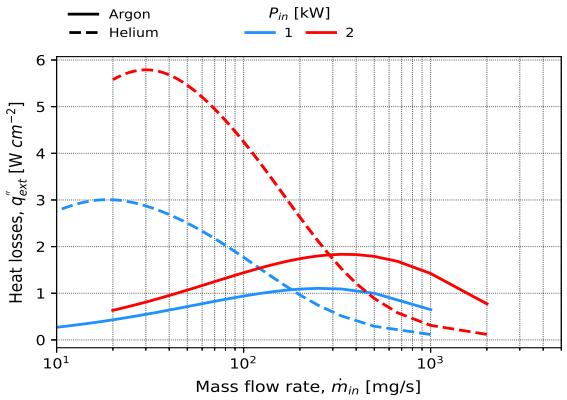

(b) Helium plasma.

Figure 3: Absorbed power density (Figure 3a) and heat transferred to the external environment (Figure 3b) for input power $1 - 5\,kW$.

DOI: 10.13009/EUCASS2025-605

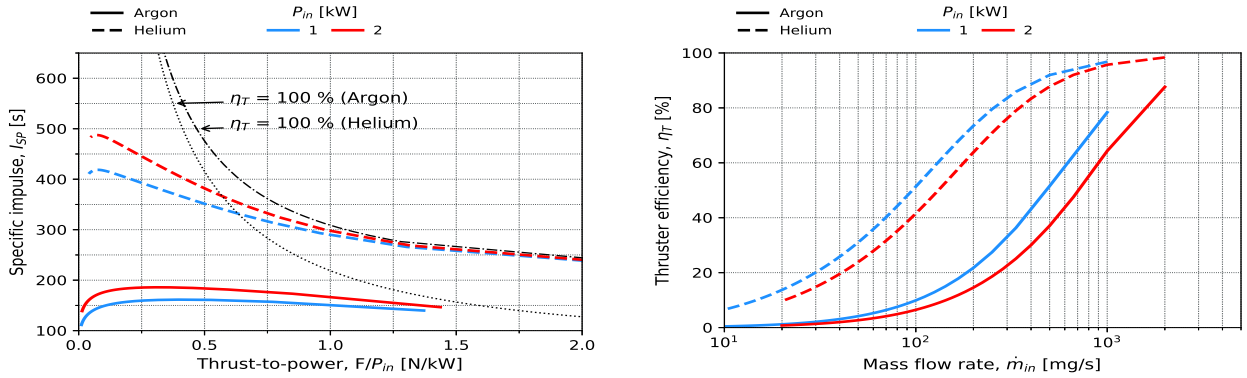

(a) Thrut-to-Power vs Specific Impulse

(b) Thruster efficiency.

Figure 4: Computed thruster performance of the argon-fed (solid line) and helium-fed (dashed line) MET. In Figure 4a, dotted and dash-dotted black line are computed assuming a thruster efficiency of 100 % in argon and helium, respectively.

monotonic behavior of the plasma losses, which cause a non-monotonic behavior of the propellant temperature curve[1]. Moreover, Figure 4a also includes the curves computed assuming an ideal thruster efficiency of 100 % (the black dotted and dash-dotted lines). As expected, the actual curves lie below these ideal one because of power losses in the plasma discharge. Finally, the specific impulse increases with input power because of enhanced propellant heating. Figure 4b displays the thruster efficiency. This performance parameter increases monotonically with mass flow rate and is consistently larger in helium than in argon because of the higher absorbed plasma density.
Overall, the helium-fed MET demonstrates the best performance, achieving specific impulse of approximately 500 s and thruster efficiency exceeding 50 % across a wide mass flow rate range. In contrast, the argon-fed MET shows lower efficiency, remaining below 50 % for a wide mass flow rate range, primarily due to large losses occurring in the plasma.

6. Conclusion and future works

This paper presented an improved global (i.e., volume-averaged) plasma model for the Microwave Electrothermal Thruster, applicable to argon and helium gases. The model computes steady-state plasma species densities and temperatures, which are then used to evaluate thrust, specific impulse, and thruster efficiency.
The approach aims at overcoming the long computational times associated with multi-dimensional fluid models, enabling rapid analyisis of the MET performance and plasma parameter across a wide range of mass flow rate. In particular, computational times remained below 1 minute.
Model results indicate that helium has the best performance, with a predicted specific impulse of approximately 400 s and efficiency exceeding 50 % at high mass flow rate. Moreover, the argon plasma shows significant power reflection, being likely the major source of inefficiency. However, except at very high flow rate, heat lost to the external environment is larger in helium, leading to high wall temperatures, close to the melting point of stainless steel.
It should be emphasized that the results of this model are purely indicative of general trends and should not be regarded as exact.
Future modeling activities should aim at extending the model to more complex molecular propellants, with a comprehensive plasma chemistry, such as nitrogen and oxygen. Finally, the influence of different wall materials should also be studied to understand the impact on discharge behavior and thruster performance.

Acknowledgements

The authors thank D-Orbit s.p.a. for supporting this work.

[1]For the sake of brevity, this curve is not reported here but it has a trend similar to the wall temperature curves showed in Figure 2.

DOI: 10.13009/EUCASS2025-605

References

[1] L. L. Alves, A. Bogaerts, V. Guerra, and M. M. Turner. Foundations of modelling of nonequilibrium low-temperature plasmas. *Plasma Sources Sci. Technol.*, 27(2):023002, 2018.

[2] T. L. Bergman, A. S. Lavine, F. P. Incropera, and D. P. DeWitt. *Fundamnetal of Heat and Mass Transfer*. John Wiley and Sons, Ltd, 8 edition, 2018.

[3] J. A. Bittencourt. *Fundamentals of Plasma Physics*. Springer-Verlag, New York, 3 edition, 2004.

[4] F. J. Bosi. Global model of microwave plasma assisted n2o dissociation for monopropellant propulsion. *Phys. Plasmas*, 26(3):033510, 2019.

[5] J. E. Brandenburg, J. Kline, and D. Sullivan. The microwave electro-thermal (met) thruster using water vapor propellant. *Plasma Sources Sci. Technol.*, 33(2):776–782, 2005.

[6] E. E. Capalungan, M. M. Micci, and S. G. Bilen. The design and development of a 30-ghz microwave electrothermal thruster. In *32rd International Electric Propulsion Conference, Wiesbaden, Germany*, 2011.

[7] D. Clemens, M. M. Micci, and S. Bilen. Microwave electrothermal thruster using simulated hydrazine. In *42nd AIAA/ASME/SAE/ASEE Joint Propulsion Conference and Exhibit*, 2006.

[8] K. D. Diamant, B. L. Zeigler, and R. B. Cohen. Microwave electrothermal thruster performance. *J. Propul. Power*, 23(1):27–34, 2007.

[9] A. Hurlbatt, A. R. Gibson, S. Schroter, J. Bredin, A. P. S. Foote, P. Grondein, D. O'Connell, and T. Gans. Concepts, capabilities, and limitations of global models: A review. *Plasma Process. Polym.*, 14(1–2):1600138, 2017.

[10] M. Lauriola and M. Nava. Feasibility study of a highe performance microwave electrothermal thruster. Master's thesis, Politecnico di Milano, 2023.

[11] J. Lee and L. L. Raja. Computational study of a helium-propellant microwave electrothermal thruster. *J. Appl. Phys.*, 135(17):173304, 2024.

[12] Dan Lev, Roger M. Myers, Kristina M. Lemmer, Jonathan Kolbeck, Hiroyuki Koizumi, and Kurt Polzin. The technological and commercial expansion of electric propulsion. *Acta Astronautica*, 159:213–227, 2019.

[13] M. A. Lieberman and A. J. Lichtenberg. *Principles of Plasma Discharges and Materials Processing*. John Wiley and Sons, Ltd., 2005.

[14] Stephane Mazouffre. Electric propulsion for satellites and spacecraft: established technologies and novel approaches. *Plasma Sources Sci. Technol.*, 25(3):033002, 2016.

[15] M. M. Micci, S. G. Bilen, and D. E. Clemens. History and current status of the microwave electrothermal thruster. In *EUCASS Proceedings Series - Advances in Aerospace Sciences*, volume 1, pages 425–438, 2009.

[16] S. T. Mousavi, E. A. D. Carbone, A. J. Wolf, W. A. Bongers, and J. van Dijk. Two-temperature balance equations implementation, numerical validation and application to h2oâhe microwave induced plasmas. *Plasma Sources Sci. Technol.*, 30(7):075007, 2021.

[17] D. Staab, A. Frey, A. Garbayo, L. Shadbolt, T. Baxter, S. Reeve, D. Hoffman, and A. Grubisic. Xmet: Design and early testing of a xenon microwave electrothermal thruster. In *36th International Electric Propulsion Conference, Vienna, Austria*, 2019.

[18] D. J. Sullivan and M. M. Micci. Development of a microwave resonant cavity electrothermal thruster prototype. In *23rd International Electric Propulsion Conference, Seattle, USA*, volume 1, pages 338–354, 1993.

[19] G. P. Sutton and O. Biblarz. *Rocket Propulsion Elements*. A Wiley Interscience publication. John Wiley and Sons, Ltd., 9 edition, 2017.

[20] M. S. Yildiz and M. Celik. Global energy transfer model of a microwave electrothermal thruster operating with helium propellant at 2.45-ghz frequency. *IEEE Trans. Plasma Sci.*, 45(8):2314–2322, 2017.

DOI: 10.13009/EUCASS2025-605

[21] M. S. Yildiz and M. Celik. Numerical investigation of the electric field distribution and the power deposition in the resonant cavity of a microwave electrothermal thruster. *AIP Advances*, 7(4):045021, 2017.

[22] M. S. Yildiz, U. Kokal, and M. Celik. Preliminary thrust measurement results of the bustlab microwave electrothermal thruster. In *53rd AIAA/SAE/ASEE Joint Propulsion Conference*, 2017.

[23] M. S. Yildiz and M. Celik M. Global energy transfer model of microwave induced plasma in a microwave electrothermal thruster resonant cavity. In *34th International Electric Propulsion Conference and 6th Nanosatellite Symposium*, 2015.